Slot Antenna Performance and Signal Quality in a Smartphone Prototype

Matthew Webb, David Gibbins, and Mark Beach, *Member, IEEE*

***Abstract*—Antenna position and user grip on smartphone-like devices may lead to obstruction of radio signal paths and antenna detuning. A multiple-input–multiple-output (MIMO) outdoor propagation measurement campaign is presented, which collected data for slot antennas on a smartphone prototype. The antennas are in four positions, two polarizations, and one was obstructed due to operator grip. All MIMO links were measured within the channel's coherence time while standing, walking, and driving. We show how signal levels change due to obstruction, position, and motion and that signal fluctuations increase significantly, thus tending to impair service quality. We also examine how proximity of the operator's hand affects the antenna's radiation and input characteristics.**

***Index Terms*—Obstruction, propagation, slot antenna.**

I. Introduction

THE PHYSICAL space available on smartphones offers many possibilities for positioning antennas [1], and clearly some of these will be more prone to the effects of certain grips than others [2]. The interaction of the user's hand with the antennas on handheld devices has been a fertile research area for some years. Computational studies using finite-difference time-domain (FDTD) analyses include [3] for the pertinent case of slot antennas, with pattern measurements in [4]. Measurement of multiple-input–multiple-output (MIMO) propagation parameters in static environments with a body phantom is conducted in [5]. Outdoor MIMO measurements in [6] isolate the antenna pattern and channel-quality changes due to a body phantom holding a smartphone prototype in a "browsing stance." Similar measurements in [7] and simulations in [8] and [9] focus on spatial MIMO parameters and channel capacity.

This letter presents results from an outdoor propagation measurement campaign in which, within the channel's coherence time, we measured two polarizations, four positions, and the impact of user obstruction of slot antennas in a smartphone prototype. We show the distributions in such scenarios of: 1) signal-to-noise ratio (SNR), with clear reductions in signal quality; 2) dynamic range of SNR showing increased signal fluctuations; 3) the relative nature of these distributions in standing, walking, and vehicular settings; and 4) measurements illustrating the degradation in the slot antenna's performance due to a typical user grip.

Manuscript received September 21, 2010; accepted October 27, 2010. Date of publication November 09, 2010; date of current version November 18, 2010.

The authors are with the Centre for Communications Research, University of Bristol, Bristol BS8 1UB, U.K. (e-mail: M.W.Webb@bristol.ac.uk).

Color versions of one or more of the figures in this letter are available online at http://ieeexplore.ieee.org

Digital Object Identifier 10.1109/LAWP.2010.2090644

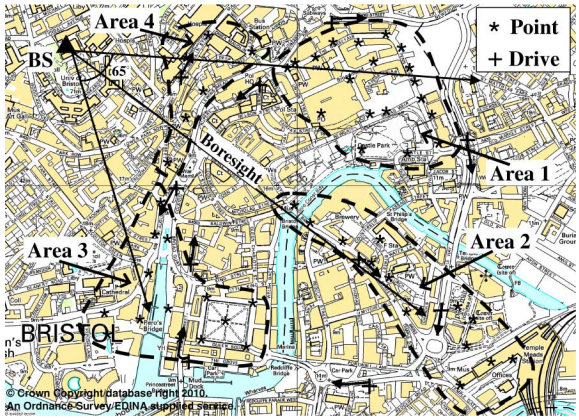

Fig. 1. Measurement locations in Bristol city-center. Scale is 1:25 000.

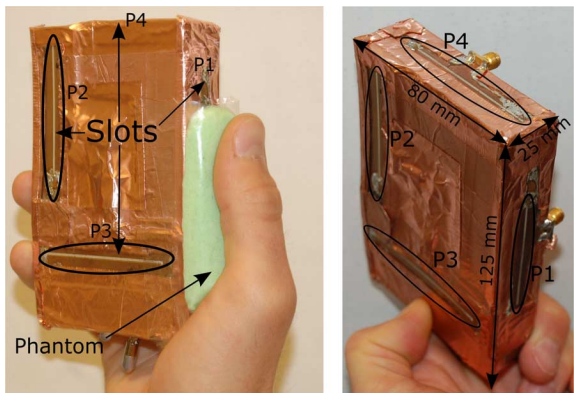

Fig. 2. Smartphone prototype, with the human grip well approximated by the position of the thumb phantom. Slot width $= 0.75$ mm, length $= 57.5$ mm.

II. Propagation Measurement Campaign

An extensive outdoor MIMO measurement campaign was carried out around Bristol city-center, U.K. [10], [11], using a multichannel wideband channel sounder [12]. The measurements were conducted at 2 GHz, with a 20-MHz signal bandwidth. The periodic transmit signal is carried through 128 discrete frequency fingers and has a repetition period of 6.4 μs. A 4×4 MIMO configuration was used throughout. Measurements were conducted at 56 point locations and along 10 drive routes shown in Fig. 1.

The measurements were conducted with a smartphone prototype of a cast aluminium box, empty inside, and sealed with copper tape. Four identical cavity-backed linear slot antennas were mounted on the prototype as shown in Fig. 2. They were positioned: 1) vertically on the right-hand side (P1); 2) in two polarizations on the body-facing plane (P2, P3); and 3) horizontally on the prototype's top rim (P4). These antennas are

discussed in detail in Section III. When in use, the human operator held the prototype in their right hand, as in Fig. 2, with his arm extended in front of his body in a typical usage stance. This inevitably obstructed the antenna on the right-hand side of the prototype. This resulted in data that measures radio propagation simultaneously in both obstructed and unobstructed slot antennas on handheld devices. The data spans a large number of measurement locations across various parts of the base-station (BS) antenna pattern, a number of different humans holding the device prototype, and includes a wide variety of propagation environments, e.g., [11].

The BS was two $\pm 45°$ dual-polarized UMTS antennas mounted on a 30-m-high building overlooking the measurement areas in the city-center. The antennas were fitted to metal railings, given 3 m horizontal separation and an 8° downtilt.

At each point location, 6 s of measurements with each device were collected while the mobile user was standing facing in each of four directions separated by successive approximate 90° rotations, followed by the user walking at 1 m/s for 6 s in each of two approximately perpendicular directions. There were 4096 samples of each frequency finger in this time. The in-vehicle measurements lasted 8.1 s each at an approximately constant speed of 30 m/h (48 k/h) and collected 7944 samples of each frequency.

III. Antenna Characteristics

In this section, we show measurements of the slot antenna's characteristics with and without obstruction by the human thumb. Results are presented for the antenna position P1 shown obstructed in Fig. 2, where the phantom placing matches the position of the thumb in a typical user grip. The other antennas are identical, so if obstructed by a different grip, they would respond similarly. These antennas are half-wavelength slots operating in their fundamental resonant mode. To approximate the thumb in pattern measurements, we replaced it with a skin-mimicking phantom with dielectric constant $\epsilon_r \approx 35$ and electrical loss of 3 dB/cm at 2 GHz. Clearly, there will be variations in how users hold the device, and the propagation measurements in Section IV cover many such possibilities.

A. Radiation Patterns

The E-plane radiation patterns of the antenna with and without the thumb phantom are in Fig. 3, with some key statistics in Table I. The patterns are normalized to the maximum value in the 3-D pattern. The phantom has little effect on the overall shape of the copolar pattern, while the relative cross-polar pattern is increased by around 5 dB and the directivity is slightly reduced. These effects are small since the phantom is in the near field of the antenna while the pattern is a far-field measurement. A much more significant effect is the reduction in maximum radiated power by 20.5 dB with the phantom. The irregularity of the pattern with the phantom is due to the power levels being closer to the noise floor in this case.

B. Input Response

In Fig. 4, there is a significant degradation in S_{11} performance with the phantom present. When radiating into free space, the antenna has a strong resonance at 2 GHz. With the application

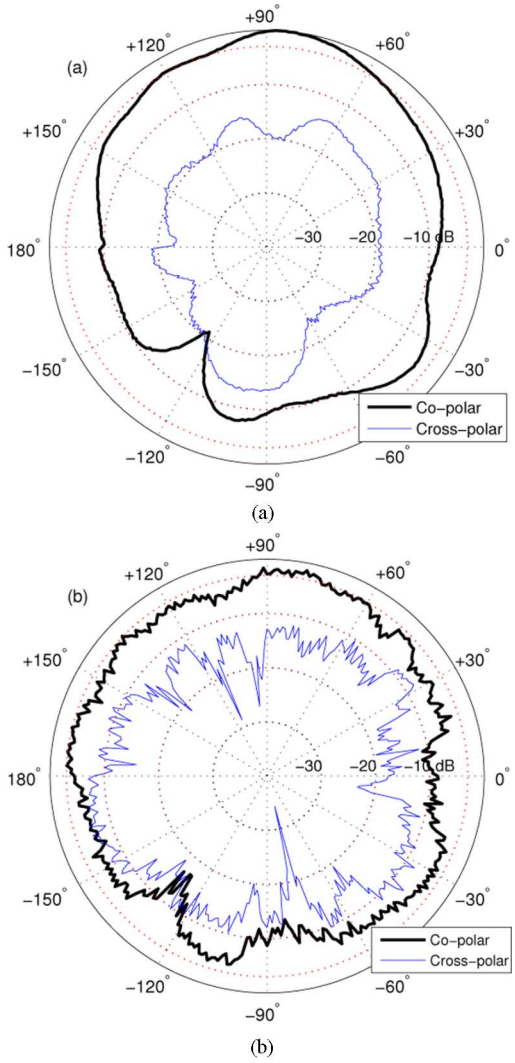

Fig. 3. Normalized E-plane polar radiation patterns of P1 (a) without and (b) with phantom in place. Maximum power level in (a) is 20.5 dB above (b).

TABLE I
Effect of Obstruction on Antenna Statistics for P1

	Free space	Phantom
Relative maximum radiated power	0 dB	-20.5 dB
Directivity	6.44 dBi	5.04 dBi
Cross polar maximum	-13 dB	-8 dB

of the phantom, the resonance disappears completely, and S_{11} worsens from -12 to -0.5 dB. This indicates that the field is no longer able to couple into the slot, due to the large reflection from the antenna substrate/phantom boundary, and suggests that the major effect is disruption of the feed point rather than alteration to the electrical size of the slot or absorption by the phantom.

Fig. 4 also compares the effects on S_{11} of the phantom and a real thumb. There is good agreement between the plots, thus validating use of the phantom in measurement. Also included is S_{11} with a layer of polythene insulator between the real thumb and the slot. There is little difference, indicating that proximity of the high-dielectric phantom, rather than shorting across the slot, is responsible for the majority of the effects.

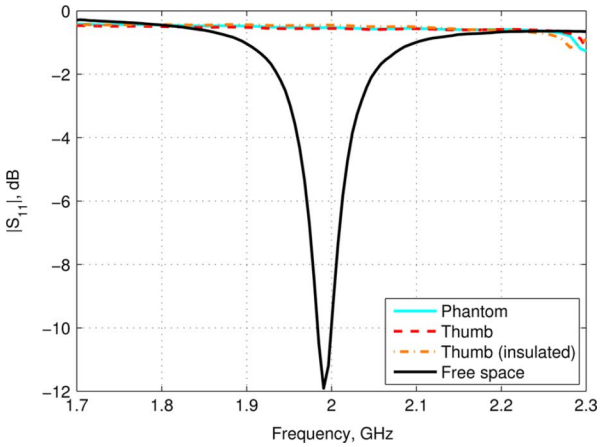

Fig. 4. S_{11} of P1 in free space, with phantom, thumb, and insulated thumb.

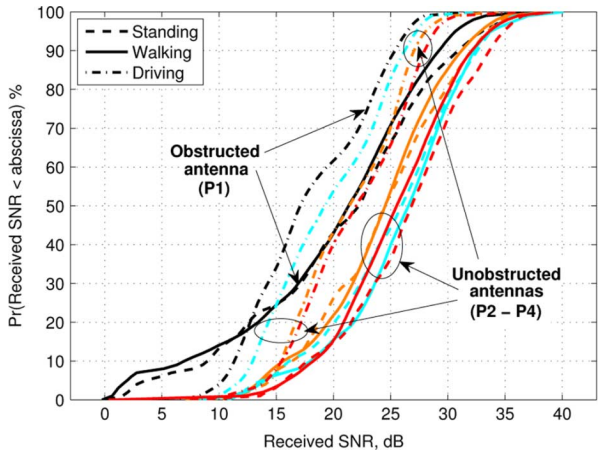

Fig. 5. Received SNR distributions of each device antenna port. Each curve color within a line style represents total received power at one antenna.

IV. Propagation Characteristics

We now analyze the 4×4 MIMO data to compare the signal quality on the obstructed and unobstructed antennas. We show results for both the 16 single-input–single-output (SISO) links and the four multiple-input–single-output (MISO) links at the receive side. We study received SNR and its dynamic range. These quantities indicate the quality and fluctuations of the received signal, with implications for quality-of-service, and the operating range devices must be designed for.

A. Calculation Methodology

As discussed in Section II, 4096 time samples of 128 frequencies were collected over 6 s for the point measurements, and 7944 over 8.1 s while driving. Consecutive sets of four samples (standing/walking) or two samples (driving) were collected within the channel's coherence time. Via an inverse Fourier transform, the 128-tap impulse response (IR) is obtained.

1) Received SNR: In a single measurement run, sets of four or two samples are within the channel's coherence time, so the variations among the IRs are due primarily to noise. Assuming this is zero-mean, coherent samples are averaged to produce one mean sample with reduced noise. This gives 1024 standing/walking or 3972 driving noise-reduced IRs.

The received signal power in one sample of one SISO subchannel is estimated by summing the power of the significant taps of the noise-reduced IR, defined as those no more than 25 dB below the peak power in the IR. Noise power at each tap is estimated as the tap's variance over the coherent samples, and total noise power in the IR is then the sum of all such noise estimates. This gives 16 SISO SNRs at each sample.

To calculate the total SNR at a receive antenna, the four received signal powers at that antenna are summed and divided by the mean of the four noise powers (since they are just multiple realizations of the same noise process). This gives four MISO SNRs at each sample.

2) Dynamic Range: Dynamic range of a given SISO or MISO channel's SNR will be defined as the difference in the decibel levels of the highest and lowest of the 1024 or 3972 SNRs found on that channel over the course of a measurement.

B. Received SNR Results

Fig. 5 shows the cumulative distribution functions (cdfs) of the received MISO SNR across the entire measurement data set. The four curves associated with each degree of mobility are the four antenna ports. It is apparent that the obstructed antennas form one set of cdfs that are at distinctly lower values than the cluster for the three unobstructed antennas. This is the case irrespective of mobility. The loss in SNR is significantly more pronounced at the lower probabilities: At the 10% level, the loss due to obstruction is some 10 dB for standing and walking, while at the 90% level it is around 3 dB—which even so represents a 50% reduction in SNR. Similarly, about 15% of SNRs are below 10 dB on the obstructed antenna, but this level is almost never reached when unobstructed. The driving SNRs are lower due to the vehicular shielding, and there is up to a 5-dB loss at 10%. Channel outage (i.e., service failure) occurs at the lower SNR levels, but these values have significantly higher probability with antenna obstruction, thus increasing the likelihood that a user will experience an outage if their signal is already poor.

At the lower percentiles, the driving SNRs are higher than walking/standing. This arises since the pedestrian measurements were sometimes in densely built areas and close to buildings, while the driving ones, being on roads, tended to be farther from their nearest physical obstructions, so the lowest SNRs occur less often.

The cdfs of the 16 SISO channels (i.e., each individual transmit–receive link) over all measurements for the walking scenario are shown in Fig. 6. The four cdfs corresponding to the obstructed antenna are again clearly to the left of the unobstructed curves. The internal grouping among the unobstructed cdfs reflects the differing characteristics of the three antennas comprising this cluster of 12 curves. The spread is widest at about 2 dB, showing that the exact positioning and polarization of an unobstructed antenna makes little difference to SNR. The same is true for the standing and driving scenarios, which are therefore omitted for clarity.

C. Dynamic Range Results

The distribution of the dynamic range of SNR on the four MISO channels is shown in Fig. 7. At the lower percentiles,

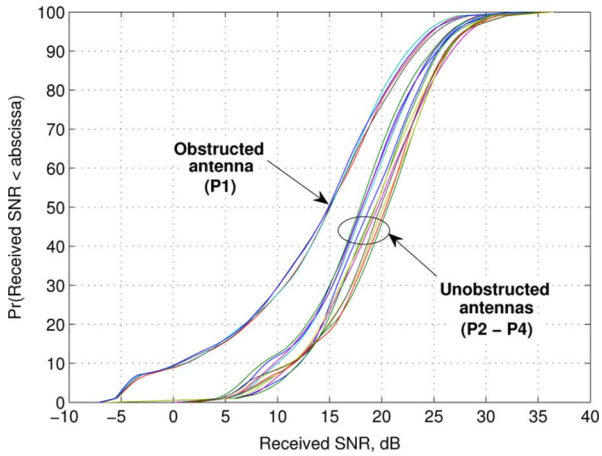

Fig. 6. Received SNR distributions of the 16 SISO subchannels: walking.

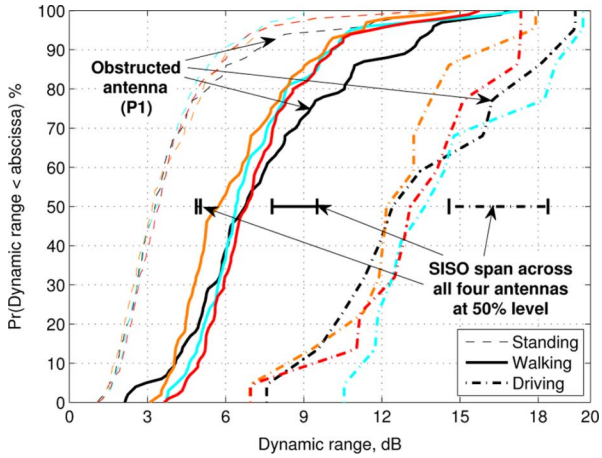

Fig. 7. Dynamic range distribution of each receive antenna port. Each curve color within a line style represents received dynamic range at one antenna.

there is little to distinguish the four antennas, particularly in the standing case. However, from the 50% level for walking and the 80% level for standing, the dynamic range is clearly larger for the obstructed antenna. For example, in the walking measurements, only 10% of cases with unobstructed antennas experience dynamic ranges above 10 dB, but more than 20% of the obstructed measurements do. The differences are smaller for the standing measurements because the fluctuations in the channel are naturally smaller if the user is static, but there is still a discernible shift to the right for the obstructed antenna. The 10-dB percentiles when standing are 1% and 5% for unobstructed and obstructed antennas, respectively. For driving, the effect of much wider propagation changes across a larger area has subsumed antenna obstruction effects; in this case, the challenges from the radio channel are the more significant.

With increased dynamic range, the performance of the device fluctuates more widely when the antenna is obstructed, which may lead to a perceived reduction in reliability. If similar losses prevail on the uplink, this could be mitigated in part by power control, but the lower absolute levels of signal power seen in Section IV-B would mean increased device transmit power and reduced battery life.

The spread of the 16 SISO dynamic ranges at the median is also indicated in Fig. 7. The effect of increased mobility is clearly seen, with the MISO ranges smaller than SISO due to the smoothing effect of transmit diversity.

V. Summary and Conclusion

An assessment of the impact of obstruction of a design of slot antenna in a smartphone prototype has been presented. Placing a thumb on the slot did not significantly alter the normalized radiation patterns, but reduced the actual sensitivity by 20 dB due mainly to disruption of the excitation. The propagation measurements showed that, irrespective of the degree of mobility, obstruction of the slot resulted in meaningful losses to signal quality and, for standing and walking users, also increased the fluctuations in the signal. This will tend to worsen a user's experience of the device as outage occurs more frequently. We have also shown that position and polarization of the slot antenna had smaller effects on signal quality than did antenna obstruction.

Acknowledgment

The authors acknowledge the partners of the Mobile VCE "MIMO Propagation Elective" for enabling collection of the propagation data. They also thank G. Hilton, W. Thompson, and M. Klemm for their help and useful discussions.

References

[1] J.-H. Choi and S.-O. Park, "Exact evaluation of channel capacity difference of MIMO handset antenna arrays," *IEEE Antennas Wireless Propag. Lett.*, vol. 9, pp. 219–222, 2010.

[2] M. Pelosi, O. Franek, M. B. Knudsen, M. Christensen, and G. F. Pedersen, "A grip study for talk and data modes in mobile phones," *IEEE Trans. Antennas Propag.*, vol. 57, no. 4, pp. 856–865, Apr. 2009.

[3] S. Dumanli, Y. Tabak, C. Railton, D. Paul, and G. Hilton, "The effect of antenna position and environment on MIMO channel capacity for a 4 element array mounted on a PDA," in *Proc. Eur. Conf. Wireless Technol.*, Manchester, U.K., Sep. 2006, pp. 201–204.

[4] K. Ogawa, H. Iwai, and N. Hatakenaka, "3D-radiation measurements of a handset diversity antenna close to a realistic human phantom in a PDA situation," in *Proc. IEEE Antennas Propag. Soc. Int. Symp.*, Columbus, OH, Jun. 2003, pp. 1029–1032.

[5] F. Harrysson, J. Medbo, A. J. Johansson, and F. Tufvesson, "Efficient experimental evaluation of a MIMO handset with user influence," *IEEE Trans. Wireless Commun.*, vol. 9, no. 2, pp. 853–863, Feb. 2010.

[6] A. Yamamoto, T. Hayashi, K. Ogawa, K. Olese, J. Ø. Nielsen, N. Zheng, and G. F. Pedersen, "Outdoor urban propagation experiment of a handset MIMO antenna with a human phantom located in a browsing stance," in *Proc. IEEE VTC, Fall*, Baltimore, MD, Sep. 2007, pp. 849–853.

[7] W. A. T. Kotterman, G. F. Pedersen, and K. Olesen, "Capacity of the mobile MIMO channel for a small wireless handset and user influence," in *Proc. IEEE Int. Symp. Pers., Indoor Mobile Radio Commun.*, Lisbon, Portugal, Sep. 2002, vol. 4, pp. 1937–1941.

[8] K. Ogawa, H. Iwai, A. Yamamoto, and J. I. Takada, "Channel capacity of a handset MIMO antenna influenced by the effects of 3D angular spectrum, polarization, and operator," in *Proc. IEEE Antennas Propag. Soc. Int. Symp.*, Albuquerque, NM, Jul. 2006, pp. 153–156.

[9] K. Ogawa, S. Amari, H. Iwai, and A. Yamamoto, "Effects of received power imbalance on the channel capacity of a handset MIMO," in *Proc. IEEE Int. Symp. Pers., Indoor Mobile Radio Commun.*, Athens, Greece, Sep. 2007, pp. 1–5.

[10] M. Hunukumbure and M. Beach, "MIMO channel measurements and analysis with prototype user devices in a 2 GHz outdoor cell," in *Proc. IEEE Int. Symp. Pers., Indoor Mobile Radio Commun.*, Helsinki, Finland, Sep. 2006, pp. 1–5.

[11] M. Beach, M. Hunukumbure, and M. Webb, "Dynamics of spatial eigen modes in measured MIMO channels with different antenna modules," in *Proc. Eur. Conf. Antennas Propag.*, Edinburgh, U.K., Sep. 2007, pp. 1–5.

[12] "RUSK channel sounder," MEDAV GmbH, Uttenreuth, Germany, 2010 [Online]. Available: http://www.channelsounder.de